X-ray absorption spectroscopy study of ReO_3 lattice dynamics

1995 J. Phys.: Condens. Matter 7 1199

(http://iopscience.iop.org/0953-8984/7/6/021)

J. Phys.: Condens. Matter 7 (1995) 1199–1213. Printed in the UK

X-ray absorption spectroscopy study of ReO_3 lattice dynamics

G Dalba†, P Fornasini†, A Kuzmin†‡, J Purans‡ and F Rocca§

† Dipartimento di Fisica, Università di Trento, I-38050 Povo (Trento), Italy

‡ Institute of Solid State Physics, University of Latvia, LV-1063 Riga, Latvia

§ Centro di Fisica degli Stati Aggregati ed Impianto Ionico del Consiglio Nazionale delle Ricerche e Istituto Trentino di Cultura, I-38050 Povo (Trento), Italy

Received 22 August 1994, in final form 14 November 1994

Abstract. The lattice dynamics of ReO_3 is studied for the first time by x-ray absorption spectroscopy (XAS) in the temperature range from 77 to 350 K at the rhenium L_3 edge. The Debye–Waller factors are extracted for the first, fourth and sixth coordination shells of rhenium, and their temperature dependences are discussed on the basis of the Debye and Einstein vibrational models. The obtained characteristic temperatures Θ_D and Θ_E are compared with the ones found by other experimental techniques. The application of the Debye and Einstein models to the analysis of the XAS and x-ray diffraction data for compounds with different degrees of correlation in atomic motion is also discussed.

1. Introduction

Rhenium trioxide (ReO_3) belongs to a wide class of perovskite-like compounds and has a simple-cubic Bravais lattice ($Pm3m$–O_h^1) with one molecule of ReO_3 per unit cell [1]. Its structure is composed of ReO_6 regular octahedra joined by corners: each rhenium atom is surrounded by six oxygen atoms, located at octahedra vertices, and each oxygen atom is linearly connected to two rhenium atoms, located at octahedra centres. The strongly anisotropic crystalline structure of ReO_3 results in a high anisotropy of vibrational and electronic properties, which have been intensively studied in the last forty years by different techniques such as Brillouin scattering [2], x-ray diffraction (XRD) [1, 3], x-ray photoelectron spectroscopy [4], Hall constant [5], nuclear magnetic resonance [6], magnetic susceptibility [7, 8], conductivity [5, 9, 10], infrared absorption [11] and ultrasonic measurements [12, 13]. It was found that physical properties of ReO_3, as well as of other perovskite-like compounds, are mainly determined by the outer d electrons of metal ions [14]. These d electrons are characterized by strong correlations and by electron–phonon coupling leading to different degrees of local lattice distortions, which can cause a phase transition due to the soft-mode instabilities [14]. However, contrary to many perovskite-like compounds, mode softening has not been found in ReO_3: this was explained by the screening effect [15].

Additional original information about ReO_3 lattice dynamics and local distortions can be obtained from the analysis of the extended x-ray absorption fine structure (EXAFS) above the Re L_3 edge [16]. Note that EXAFS is strongly sensitive to atomic correlation effects. Therefore EXAFS, together with XRD, which gives complementary information about uncorrelated atomic motion, can be used to test different models of lattice dynamics, e.g., the Einstein or Debye models [17]. In this paper we present an original EXAFS study of the temperature dependence of the Debye–Waller (DW) factors for the first, fourth and sixth coordination shells of rhenium atoms from 77 to 350 K. The results are considered on the

0953-8984/95/061199+15$19.50

basis of the Debye and Einstein models and are compared with the XRD data [3]. The meaning of the extracted characteristic temperatures is discussed in comparison with other techniques.

The paper is organised as follows: in section 2, the experimental procedure of EXAFS measurements at the Re L_3 edge in ReO_3 is described; in section 3, we discuss the origin of several contributions to EXAFS and present data treatment procedures; in section 4, the Debye and Einstein vibrational models, their asymptotic behaviour and the range of reliability are discussed; in section 5, the results are presented; in section 6, we compare our results with the ones from other experimental techniques; in section 7, the summary of the present work and the main conclusions are given.

2. Experimental details

X-ray absorption spectra of the Re L_3 edge in ReO_3 were recorded in transmission mode at the ADONE storage ring (Laboratori Nazionali di Frascati) on the PWA–BX2 beamline using the synchrotron radiation coming from the wiggler source. The storage ring ADONE operated at 1.4 GeV with the maximum stored current 60 mA and the wiggler magnetic field 1.6 T. The sample was prepared from polycrystalline ReO_3, which was finely ground and homogeneously deposited on a polytetrafluoroethylene membrane by a sonication technique. The thickness of the sample was optimized to have the value of the absorption jump $\Delta\mu x \simeq 1$ (μ is the absorption coefficient, x the sample thickness). The data were recorded with a spacing of 1 eV in the XANES (x-ray absorption near-edge structure) region and 2 eV in the EXAFS region. A standard transmission scheme [18] with a Si(111) channel-cut crystal monochromator and two ion chambers containing krypton gas was used. The sample was mounted in a liquid nitrogen cryostat with heating resistor. The temperature was varied within the range from 77 to 350 K and was stabilized within ±2 K during each measurement.

3. Data analysis

The EXAFS spectra were treated following the procedure previously described by us [19, 20]. The experimental EXAFS spectra and their Fourier transforms (FTs) are shown in figure 1. Note that the positions of peaks in the FT are shifted from their true crystallographic values because FTs were calculated without phase correction.

Five main peaks (located at 0.7–1.9 Å, 2.1–3.1 Å, 3.1–4.0 Å, 4.4–5.5 Å and 5.8–6.8 Å) are present in the FTs of experimental EXAFS spectra (figure 1(b)) [19, 21]. The first one corresponds to single-scattering processes on six oxygen (O_1) atoms forming the regular octahedron of the first coordination shell at the distance R(Re–O_1) = 1.874 Å. The second peak is attributed to multiple-scattering (MS) processes within the first shell [19, 21]. The third peak corresponds mainly to scattering from the second shell formed by six rhenium (Re_2) atoms (R(Re–Re_2) = 3.748 Å), and its amplitude is significantly influenced by the strong focusing effect due to the oxygen atoms of the first shell [19, 21]. Note that 24 oxygens (O_3), located at ~4.19 Å and forming the third coordination shell, also give some contribution to the third peak. The fourth peak corresponds mainly to the single-scattering signal from 12 rhenium (Re_4) atoms at ~5.30 Å and 30 oxygens (O_5) of the fifth shell at ~5.62 Å. The last peak (at 5.8–6.8 Å) is due to eight rhenium (Re_6) atoms located at ~6.49 Å in the ⟨111⟩ directions and 24 oxygen (O_7) atoms at ~6.76 Å.

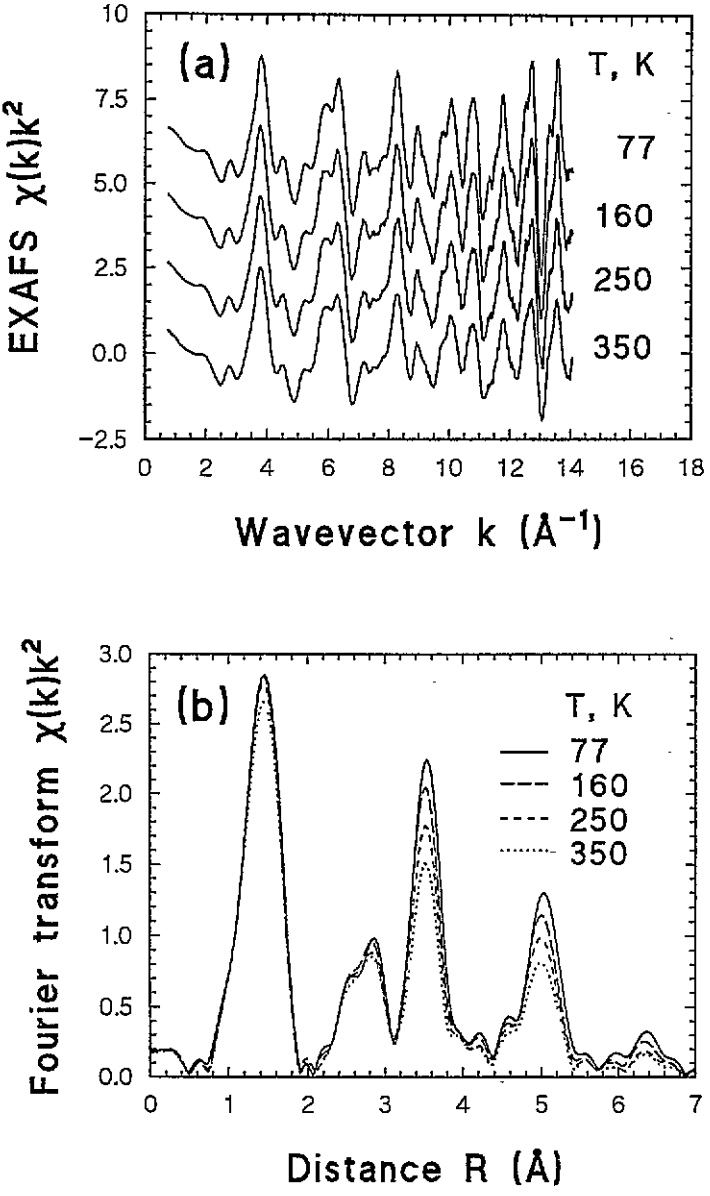

Figure 1. (a) Temperature dependence of the experimental EXAFS $\chi(k)k^2$ spectra measured at the Re L_3 edge in ReO_3. (b) Fourier transforms of the EXAFS signals shown in (a). Only four spectra are shown for clarity.

A significant decrease of peak amplitude with increasing temperature is clearly visible, especially for the peaks beyond the first one. In this paper we will analyse the variations of the amplitude of the first, fourth and fifth peaks. These peaks are well isolated and their contributions can be easily singled out by the back FT. The EXAFS signals from these shells are dominated by single-scattering processes, therefore a standard single-scattering multishell analysis can be used to extract the values of the DW factor. Moreover, although

both the fourth and fifth peaks contain the signals from two shells (rhenium and oxygen), single-shell contributions can be separated in k-space due to the large difference of rhenium and oxygen backscattering amplitudes: oxygen and rhenium atoms contribute mainly to the low-k and high-k ranges of EXAFS signal, respectively. This separability is enhanced by the large difference in the values of rhenium and oxygen DW factors (see below). The analysis of the second (2.1–3.1 Å) and third (3.1–4.0 Å) peaks, complicated by the presence of strong MS contributions, is in progress and will be published in a forthcoming paper.

The contribution from a single shell to EXAFS $\chi(k)$ for an unoriented sample is given, in the *single-scattering curved-wave* formalism and in the *harmonic* approximation, by [22, 23]

$$\chi(k) = A(k, R)\sin\Psi(k, R) = \frac{NS_0^2}{kR^2} f(k, R)\exp(-2\sigma^2k^2)\sin(2kR + \psi(k, R)) \tag{1}$$

where k is the photoelectron wavevector, $A(k, R)$ and $\Psi(k, R)$ are the total amplitude and the phase of the EXAFS signal, R is the interatomic distance, N the coordination number, S_0^2 the multielectron amplitude reduction factor, σ^2 the EXAFS DW factor, $f(k, R)$ the backscattering amplitude of the photoelectron and $\psi(k, R)$ the phase shift of the photoelectron due to absorbing and backscattering atoms. Note that the backscattering amplitude $f(k, R)$ in equation (1) includes the correction for the inelastic mean free path (MFP) $\lambda(k)$ of the photoelectron. The photoelectron wavevector k is defined as $k = \sqrt{(2m_e/\hbar^2)(E - E_0)}$, where m_e is the electron mass and $E - E_0$ is the photoelectron kinetic energy measured from the inner core photoemission threshold (vacuum level). The energy origin E_0 was located at 5 eV above the white line maximum according to the procedure utilized by us earlier [19]. The correct choice of E_0 position is essential to align experimental and theoretical spectra.

The EXAFS DW factor σ^2 has the meaning of *mean square relative displacement* (MSRD) and can be connected to vibrational properties of atoms by [17]

$$\sigma^2 = \langle[\hat{R}\cdot(u_B - u_A)]^2\rangle \tag{2}$$

where $\hat{R} = R/R$ and R is the equilibrium distance between absorbing (A) and backscattering (B) atoms, u_A and u_B are the displacement vectors of absorbing and backscattering atoms from their equilibrium positions and the angular brackets refer to a canonical average. By calculating the square in equation (2) we obtain

$$\sigma^2 = \langle(\hat{R}\cdot u_A)^2\rangle + \langle(\hat{R}\cdot u_B)^2\rangle - 2\langle(\hat{R}\cdot u_A)(\hat{R}\cdot u_B)\rangle = \langle u_A^2\rangle + \langle u_B^2\rangle - 2\langle u_A u_B\rangle \tag{3}$$

where the first two terms (we will refer to their sum as σ^2_{MSD}) are the uncorrelated *mean square displacements* (MSDs) of the two atoms and the last term $2\langle u_A u_B\rangle \equiv \sigma^2_{DCF}$ is the *displacement correlation function* (DCF). For ReO_3, we will consider three pairs of atoms (Re, O_I), (Re, Re_4) and (Re, Re_6) respectively for the first, fourth and fifth peaks. The oxygen and rhenium MSDs were determined by temperature-dependent XRD measurements [3].

The DW factors can be obtained from the analysis of EXAFS spectra using scattering amplitudes calculated theoretically or extracted from a reference experimental EXAFS spectrum. The first approach gives *absolute* DW factor values but the reliability of calculated scattering amplitudes has to be verified. Experimental scattering amplitudes obtained from a low-temperature spectrum of the studied compound are generally more accurate but only

relative DW factor values can be determined in this case. Moreover, the two methods are differently affected by experimental data noise. The comparative use of both methods can be of great help to obtain at the same time accurate and absolute DW factor values. With this aim, a good criterion is the coincidence of the slopes for the two DW factor temperature dependences (absolute and relative).

The DW factor values σ^2, reported in this work for the first peak in figure 1(b) (first coordination shell, Re–O), were found using the three different methods described below; only the first and third methods were used in the analysis of the fourth and fifth peaks. The methods are as follows.

(1) Least-squares fit of the $\chi(k)k^2$ signal using equation (1) with the backscattering amplitude, $f_{th}(k, R)$, and phase shift, $\psi_{th}(k, R)$, calculated by the FEFF3 code [24, 25]. Since the energy origin of the photoelectron E_0 is defined in the FEFF3 code relative to the Fermi level E_F [25], and our choice is the vacuum level E_v [19], the energy scale of $f_{th}(k, R)$ and $\psi_{th}(k, R)$ was corrected by the work function $\phi = E_v - E_F$ [26] to have the same energy origin as the experimental EXAFS $\chi(k)$.

(2) Least-squares fit of the $\chi(k)k^2$ signal using equation (1) with experimental amplitude $f(k, R) = f_{77}(k)$ and phase shift $\psi(k, R) = \psi_{77}(k)$ extracted from the experimental spectrum measured at 77 K, assuming $N_{77} = 6$ and $R_{77} = 1.8737$ Å [27].

(3) The amplitude analysis [22] relative to the experimental data measured at 77 K

$$\ln \frac{A_T}{A_{77}} = \ln \frac{N_T R_{77}^2}{N_{77} R_T^2} - 2k^2(\sigma_T^2 - \sigma_{77}^2) \tag{4}$$

where A_T is the amplitude of the EXAFS signal measured at temperature T. The A_T were determined by the back FT of the peaks, shown in figure 1(b), in the ranges 0.7–1.9 Å, 4.4–5.5 Å and 5.8–6.8 Å for the first, fourth and fifth peaks, respectively. The k-space analysis was done from 2–4 $Å^{-1}$ to 13 $Å^{-1}$. In both the fourth and fifth peaks, in addition to the contribution from rhenium atoms, there is also a contribution from oxygen atoms. However this method, which is generally applicable only to the single-shell analysis, gives values of DW factors for the Re–Re atom pairs whose temperature dependence agrees well with the one obtained by the first method. The reason is that the relatively light oxygen atoms, located at long distances in the outer shells, have a very large DW factor as compared to those of the heavier rhenium atoms, therefore their contribution to the EXAFS signal decreases so rapidly with increasing energy that only the rhenium contribution is significant at $k > 4$ $Å^{-1}$. Note that the equation (4) was derived in the harmonic approximation, and in the case of an anharmonic contribution, additional terms appear in (4). In the present work, we checked the possible presence of anharmonic effects using a cumulant approach [22, 28]. No such contributions were found, within experimental error, at $T < 350$ K.

Since methods (2) and (3) give only relative DW factor values, to get absolute values, data were shifted upward so as to reach the best agreement between the slope of their temperature dependence and one of a vibrational model, e.g., Einstein or Debye [22].

In addition to the information on DW factors, the temperature variation of the Re–O_1 distance was estimated. Our analysis of the EXAFS spectra using the best-fit procedure of $\chi(k)k^2$ signals (method (2)) and the comparison of experimental phases [22] shows that Re–O distance remains constant in our range of temperatures with an accuracy ±0.001 Å. This is in good agreement with temperature-dependent XRD lattice-constant measurements [27], giving the variation of the distance $\Delta R_{XRD} = R_{350} - R_{77} = (3.0 \pm 0.5) \times 10^{-4}$ Å.

4. Vibrational models

In this section the Debye and Einstein vibrational models for the calculation of MSRD and MSD are considered [17, 29, 30], and the range of their reliability is estimated from asymptotic behaviour.

The correlated Debye model, developed for *high-symmetry monatomic* systems, is based on a spherically averaged projected density of vibrational states

$$\rho_R(\omega) = \frac{3\omega^2}{\omega_D^3}\left[1 - \frac{\sin(\omega R q_D/\omega_D)}{\omega R q_D/\omega_D}\right] \tag{5}$$

where $\omega_D = k_B\Theta_D/\hbar$ is the Debye frequency, $q_D = (6\pi^2 N_0/V)^{1/3}$ is the Debye wavevector. The second term in square brackets describes correlation effects.

The Einstein model is obtained by considering a delta-shaped density of vibrational states

$$\rho_R(\omega) = \delta(\omega - \omega_E) \tag{6}$$

where ω_E is the Einstein frequency.

The asymptotic behaviour at $T \to 0$ and $T \to \infty$ of the correlated and uncorrelated Debye models in comparison with the Einstein model represents special interest for further speculations on their reliability and accuracy for use in the EXAFS analysis. If one requires that the DW factors calculated with Debye and Einstein models have the same behaviour at high temperatures (as expected within harmonic approximation), the relations between Einstein Θ_E and Debye Θ_D characteristic temperatures are

$$\Theta_E = \Theta_D/\sqrt{3} \qquad \text{for MSD} \tag{7}$$

$$\Theta_E = \Theta_D/\sqrt{3S} \qquad \text{for MSRD} \tag{8}$$

with

$$S = \sum_{n=1}^{\infty} \frac{(q_D R)^{2n}(-1)^{n+1}}{(2n+1)(2n+1)!}.$$

While both models give the same linear asymptotic behaviour of MSD and MSRD at high temperatures, a non-negligible difference can be found at low temperatures. In figure 2 we compare the behaviour of Einstein and Debye models whose characteristic temperatures are connected through the asymptotic equations (7) or (8) for MSD or MSRD, respectively; two Debye temperatures are considered, 400 and 800 K. The MSDs are very similar except at very low temperatures, typically below liquid nitrogen temperature. A different behaviour is found for the MSRDs. Einstein and correlated Debye models can give MSRDs significantly different also at relatively high temperatures, particularly for small $q_D R$ values. Note that the Einstein model tends to overestimate the MSD and MSRD values at low temperatures in comparison with the Debye model.

The relative merit of the two models in interpreting the EXAFS data depends on the specific problem to be solved. The Einstein model has been used for molecular systems (gases and molecular crystals). The correlated Debye model has been used for metals. On more general grounds it is thought that the Einstein model better describes the vibrational effects due to dispersionless optical branches, while the Debye model better describes the

effect of long-wavelength acoustic modes. Both kinds of mode are generally present in non-Bravais crystalline compounds.

The Einstein frequency obtained by best fitting the EXAFS DW factors depends on coordination shell; it is a measure of an 'effective' bond-stretching force constant $K = \mu\omega_E^2$ taking into account the effect of all vibrational modes within the first BZ (μ is the reduced mass of the absorber–backscatterer pair). Only in particular cases (e.g., molecular crystals) does it correspond to actual frequencies of optical branches.

The correlated Debye model aims at describing the MSRDs by one Debye frequency (to be correlated to Debye frequencies obtained from other techniques); the variations of MSRD with interatomic distance depend on a geometrical factor $q_D R$. This model actually can fail also for relatively simple systems such as germanium, for which different Debye frequencies have to be used for different coordination shells.

5. Results

The Debye model was developed for *monatomic* and *isotropic* systems by replacing the three acoustic branches of the vibrational spectrum with three branches having the same linear dispersion relation [26]. Rhenium trioxide is a highly anisotropic polyatomic crystal with four atoms (one rhenium and three oxygens) in the cubic unit cell ($a = 3.748$ Å) and then has 12 vibrational branches (three acoustic and nine optical). Moreover, the atomic masses of rhenium and oxygen are very different, $M_{Re} = 186.2$ amu and $M_O = 15.999$ amu. The reduced masses of the Re–O and Re–Re pairs are equal to 14.73 amu and 93.10 amu, respectively. The application of the Debye model to rhenium trioxide requires the use of some relevant approximations. We have considered an 'extended' BZ approach [26] where (1) the contribution of nine optical and three acoustic branches was approximated by three linear branches and (2) the sum over the first BZ was replaced by an integral over the Debye sphere of radius $q_D = 1.65$ Å^{-1} with the volume being four times the volume of the first BZ.

The temperature dependences of the MSRD obtained from EXAFS, and of the MSD calculated from XRD data [3] as a sum of individual MSDs of two atoms, were fitted by the Einstein model and by the correlated and uncorrelated Debye models. Only one free parameter Θ_E or Θ_D was used for MSD and for MSRD extracted by the first method (see section 3). In the case of the MSRD obtained by the second and third methods, giving relative values, two free parameters were used: the first one is the characteristic temperature and the second one is a constant allowing an upward shift of the experimental points to match the model. The DW factors, obtained by methods (2) and (3) of section 3, are in good agreement, therefore from now on we will refer to their average values when speaking of relative MSRD.

The results of the fitting procedure are shown in figure 3. The obtained values of the characteristic temperatures Θ_D and Θ_E for the first (O_1), fourth (Re_4) and sixth (Re_6) coordination shells are presented in table 1. The additional dotted curves in figure 3(a) correspond to the uncorrelated and correlated Debye models for the Re–O_1 atom pair with $\Theta_D = 780$ K, which is the average value calculated from the MSD and the absolute MSRD data and consistent with both sets of data within the error bar. The error bars of Θ in table 1 are related to the error bars of the DW factors. Note that errors for first shell are larger than the ones for outer shells due to the flatter behaviour of the DW factor temperature dependence of the first shell.

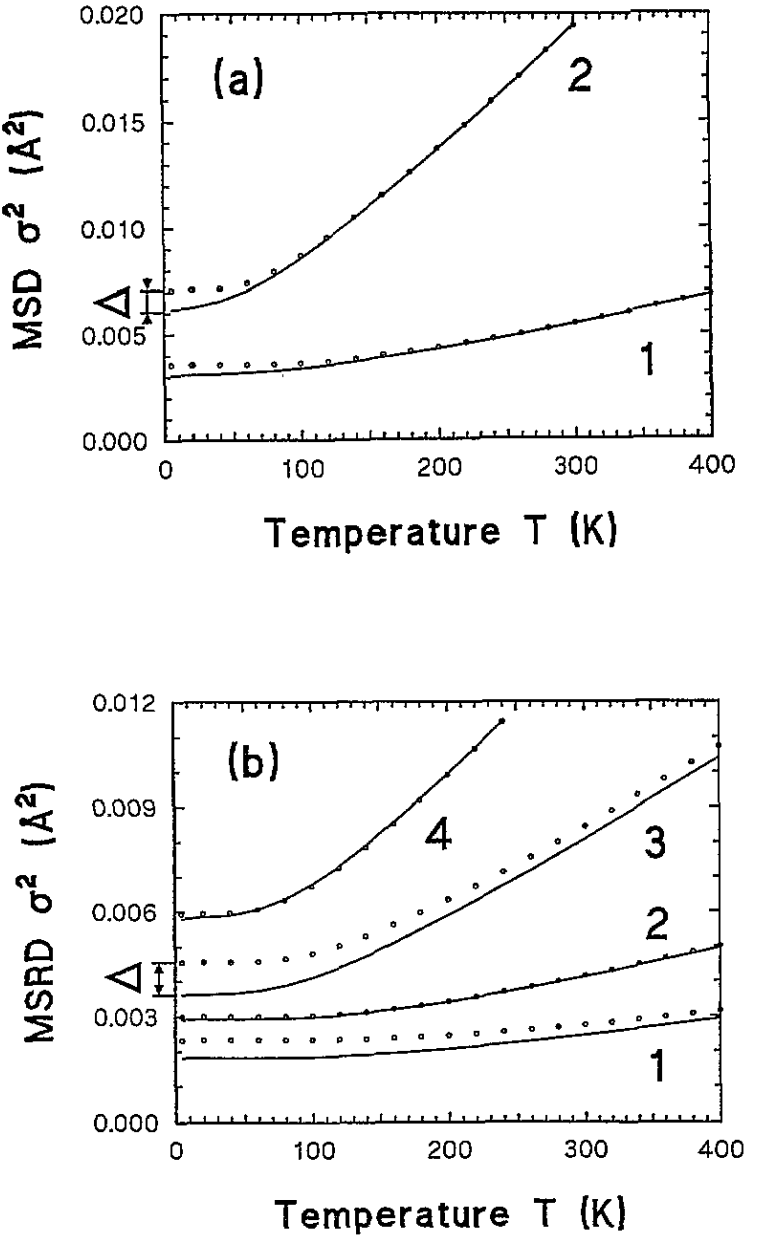

Figure 2. Comparison of the Einstein model (circles) with (a) uncorrelated and (b) correlated Debye models (solid line). The Debye and Einstein models are aligned one to another at high temperatures. The values of Θ_E were calculated from Θ_D using equation (7) in (a) and (8) in (b). The parameters of the models are (a) $\Theta_D = 800$ K, $\Theta_E = 462$ K (curves 1) and $\Theta_D = 400$ K, $\Theta_E = 231$ K (curves 2), (b) $\Theta_D = 800$ K, $q_D R = 3.0$ and $\Theta_E = 729$ K (curves 1), $\Theta_D = 800$ K, $q_D R = 5.0$ and $\Theta_E = 556$ K (curves 2), $\Theta_D = 400$ K, $q_D R = 3.0$ and $\Theta_E = 364$ K (curves 3), $\Theta_D = 400$ K, $q_D R = 5.0$ and $\Theta_E = 278$ K (curves 4).

Table 1. Best-fit values of the characteristic Einstein Θ_E and Debye Θ_D temperatures (in K) obtained from temperature dependences of σ^2_{MSD} and σ^2_{MSRD} for the first (O_1), fourth (Re_4) and sixth (Re_6) coordination shells. For the Einstein model, the values of Θ_E, calculated from Θ_D by equations (7) and (8), are shown in square brackets.

Shell	Model	Θ (MSD)	Θ (MSRD) (first method)	Θ (MSRD) (second and third methods)
1	Debye	760±20	805±30	850±60
	Einstein	444±20 [439]	822±30 [734]	719±60 [775]
4	Debye	360±10	333±20	343±20
	Einstein	207±10 [207]	214±20 [213]	219±20 [220]
6	Debye	360±10	360±20	340±20
	Einstein	207±10 [208]	227±20 [225]	210±20 [213]

Very different characteristic Debye temperatures obtained from the MSRDs have been found for the first (~800 K) and the outer (~350 K) shells: this reflects the large difference in the effective strength of interactions between atoms in the Re–O and Re–Re pairs.

As one can see from table 1, the relation between Θ_D and Θ_E values agrees well with the one predicted by equation (7) for MSDs; for MSRDs the agreement with the prediction of equation (8) is good for the fourth and sixth shells ($q_D R = 8.7$ and $q_D R = 10.7$, respectively), less satisfactory for the first shell ($q_D R = 3$). This result is consistent with the discussion of section 4 (figure 2). From experimental results it is however impossible to decide on the relative merit of the two models, in view of the uncertainties to be discussed here below. The low values of Θ obtained for the fourth shell in comparison with the sixth one (table 1) indicate the level of uncertainty of the whole procedure. The average values $\Theta_D = 344\pm20$ K and $\Theta_E = 218\pm20$ K will be used for these two shells in the following. The relatively large differences between Θ_D (or Θ_E) values for the first shell, obtained from absolute and relative MSRDs, are due to the flat behaviour of the first-shell MSRD temperature dependence that leads to large uncertainty of fitting parameters when their number is more than one (as in the case of the relative MSRD). Moreover, the error bars of both the Debye and Einstein temperatures for the relative DW MSRD in the first shell (see table 1) are very large. Therefore, taking into account the last result and the fact that the temperature dependence of the relative MSRD matches well the absolute one, only the set of the absolute MSRDs will be considered further.

Let us consider the behaviour of the displacement correlation function (DCF) equal to the difference between MSRD and MSD [17]. The DCF is large for the first shell (it is more than 40% at 77 K and grows with temperature), but it decreases rapidly for outer shells reflecting the decrease of correlation in atomic motion of distant atoms (figure 3). A good estimate of the correlation can be the ratio $\gamma = \sigma^2_{DCF}/\sigma^2_{MSD}$ of DCF to MSD [30] shown in figure 4: $\gamma = 1$ for completely correlated motion and $\gamma = 0$ in the opposite case.

The reasons for the high correlation of atomic motion of rhenium and oxygen nearest neighbours in ReO_3 are the strength of the Re–O bond and the large difference of atomic masses of rhenium and oxygen atoms, as will be discussed in the following. The presence of strong correlation of atomic motion for the nearest-neighbour rhenium and oxygen atoms confirms the result of elastic constant measurements showing that the acoustic properties of ReO_3 are dominated by very strong Re–O bonds [2, 12, 13].

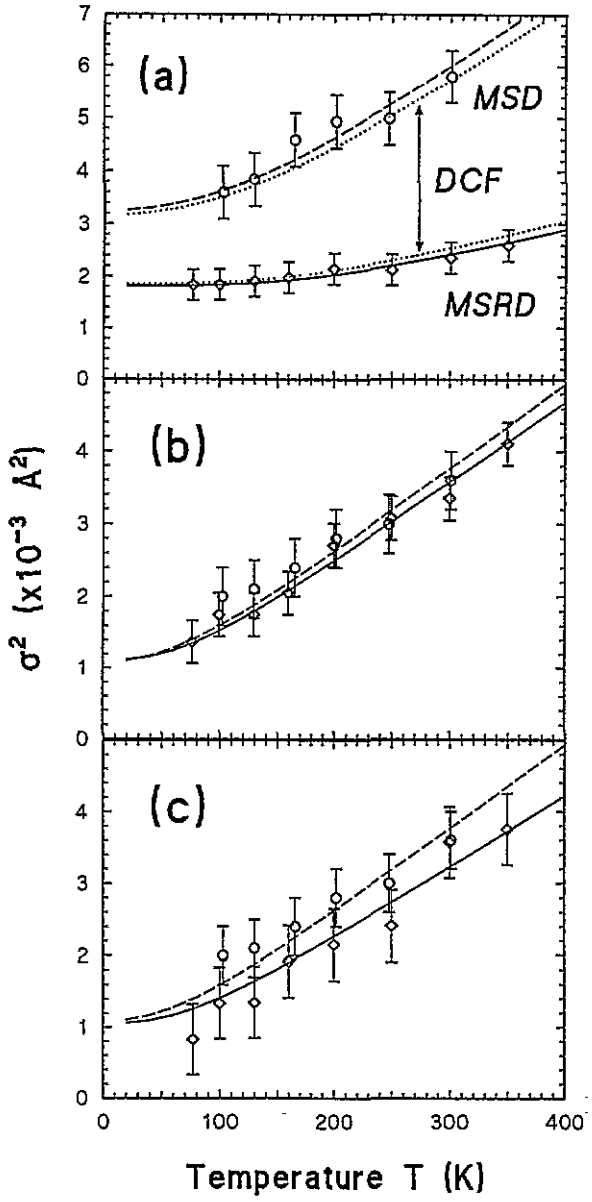

Figure 3. Temperature dependence of the MSDs (circles), found by XRD in [3], and MSRDs (diamonds), obtained by EXAFS in present work, for (a) Re–O_1, (b) Re–Re_4 and (c) Re–Re_6 atom pairs in comparison with the uncorrelated (dashed line) and correlated (solid line) Debye models calculated with Θ_D taken from columns three and four of table 1. The uncorrelated and correlated Debye models with $\Theta_D = 780$ K is shown by the dotted lines in (a).

6. Discussion

The phonon spectrum of ReO_3 [31] can be roughly divided into two parts, related to acoustic and optical modes respectively: below and above $\omega = 260$ cm^{-1}. The optical bond-stretching modes (Re–O) are observed in the region from 920 cm^{-1} to 600 cm^{-1} and

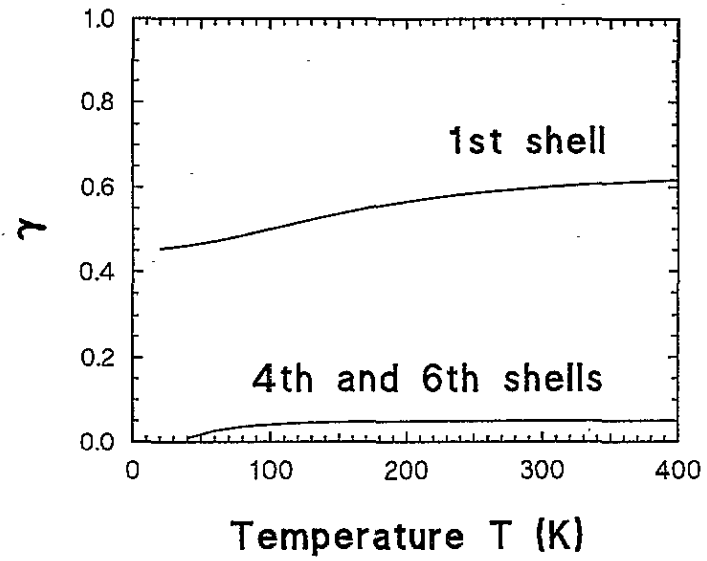

Figure 4. Ratio γ [30] of DCF to MSD, estimating the degree of correlation, as a function of temperature for the first, fourth and sixth shells in ReO_3. ($\gamma = 0$ corresponds to uncorrelated motion.)

those assigned to the angle-bending modes (O–Re–O) are observed below 450 cm^{-1} [11, 13]. These modes have been probed together or separately by different techniques such as acoustic [12, 13], electric conductivity [9, 10] and specific heat [8, 9] measurements, inelastic neutron [32] and Brillouin scattering [2], infrared (IR) absorption and Raman spectroscopies [11]. Their results are briefly summarized below and discussed in comparison with the ones given by EXAFS and XRD.

EXAFS and XRD allow us to partly separate the contributions of acoustic and optical phonons by looking at the atoms located in different coordination shells. As has been shown in a model study of diatomic chains with very different atomic masses [33], the contribution of optical phonons to the first-shell MSRD dominates in the low-temperature region because of large zero-point vibration, whereas the acoustic phonons give a dominant contribution to the MSRD of the heavy-atom pairs (next shells). Moreover, optical phonons are not excited in the low-temperature region and the MSRD of the first shell shows very small temperature dependence [33], whereas acoustic phonons are easily excited even at low temperature and significantly contribute to the MSRD of the heavy-atom pairs. The temperature dependences of the MSRD shown in figure 3 are in good agreement with the proposed model [33]. In particular, the DW factor of Re–O atom pairs reflects optical stretching vibrations, while the DW factor of the distant-located rhenium atoms is characterized by long-wavelength acoustic vibrations. Thus, analysing the temperature behaviour of the DW factor of the first and the outer shells, the characteristic temperatures related to different parts of the phonon density of states can be extracted (table 1).

Phonon-dispersion curves for ReO_3 were first calculated using the *valence-field* model [11]. The results show that the phonon spectrum of ReO_3 has a wide gap, separating three high-frequency optical stretching modes from the others. However, in the frame of the *valence-field* model, the ReO_3 lattice is unstable for some modes with the wavevector in the points M and R of the BZ. In perovskite-type compounds, such modes, corresponding to the rotational motion of oxygens around a metal ion, lead to phase transitions which has not

been found in ReO_3. This problem has been solved by the use of the *rigid-ion* model taking into account the electrostatic interaction [31]: in this case, the ReO_3 lattice does not show instability. In the total one-phonon density of states in ReO_3, calculated in the framework of the rigid-ion model, there are three separate regions related to three acoustic modes, six low-frequency optical modes and three high-frequency optical modes.

The direct observation of optical phonons, at the centre of the BZ ($q = 0$), was made by IR spectroscopy [11]. Two peaks were found at room temperature at 905 and 315 cm^{-1} and assigned to several optical vibrational modes [11]: three corresponding to the Re–O bond stretching modes, and three corresponding to the O–Re–O bending modes, which are in agreement with the second-order Raman spectrum. There are also three low-frequency optical bending modes which are inactive in IR spectra. These results and the temperature dependence of electric conductivity [11] were interpreted by an Einstein model with $\Theta_E = 800$ K and optical phonons at 555 cm^{-1}. These data are in good agreement with the last studies of the electric conductivity of ReO_3 as well [34].

The IR and Raman spectroscopy studies of tungsten oxides with ReO_3-type structures confirm that the M–O–M stretching and bending modes are expected at 700 and 300 cm^{-1} respectively [35, 36]. Also the inelastic-neutron-diffraction studies of the isostuctural perovskite-like tungsten bronze and tungsten trioxides show broad peaks at about 500 cm^{-1} assigned to M–O framework vibrations [37].

The Einstein temperatures reported in the literature [9–11, 34–37] are in reasonable agreement with those obtained from the first-shell MSRD (table 1). The difference between the Einstein temperatures obtained from the first-shell MSRD and MSD is due to the fact that the MSD of the Re–O pair contains both optic and acoustic contributions; this yields a lower Einstein temperature.

The projected density of states can be also approximated by the Debye model. We found that in ReO_3 the temperature dependence of the MSD, given by XRD, and the MSRD, given by EXAFS, in the outer coordination shells can be well approximated by the uncorrelated and correlated Debye models, respectively, with close characteristic temperatures (table 1). The reason for the large difference between the first- and outer-shell Θ_D values is the strong rhenium–oxygen bond leading to a high correlation of atomic motion in the first shell (figure 4).

Table 2. Characteristic Debye temperatures related to the acoustic phonons in ReO_3.

Method	Θ_D (K)
Ultrasonic measurements	528 [12], 544 [13]
(corrected in this work)	322–345 [12, 13]
Brillouin scattering	560 [2]
Conductivity	327 [9], 330 [10], 460 [12], 450 [34]
Low-temperature specific heat	327 [9], 460 [8]
X-ray diffraction (Re–Re pairs)	360 [3]
EXAFS (Re–Re pairs)	344–360 (this work)
Rigid-ion model	374 [31]

The characteristic temperatures and the experimental techniques, which are more sensitive to acoustic phonons, are listed in table 2. Here the values of Θ_D, given by XRD and EXAFS, have been obtained from the temperature dependences of MSD and MSRD for the outer (fourth and sixth) shells consisting of rhenium atoms. Note that in ReO_3, where the atomic masses of Re and O atoms are very different, the maximum frequency

of acoustic modes depends only on the mass of rhenium. As one can see, there is a quite good agreement between different experimental methods and the result of the calculation based on the rigid-ion model [31], which gives the cut-off frequency of the acoustic modes ~260 cm^{-1} (~374 K).

ReO_3 is a metallic compound therefore the temperature dependence of its electric conductivity is closely related to the lattice thermal vibrations. In particular, the resistivity of ReO_3 shows well expressed non-linear dependence on temperature in the range from 4.2 to 300 K [5, 9, 10, 34]. Its analysis in terms of electron scattering both by acoustic and optical phonons was done within the Debye (Θ_D = 327 K [9], Θ_D = 330 K [10], Θ_D = 450 K [34]) and Einstein (Θ_E = 1080 K [9], Θ_E = 800 K [10], Θ_E = 900 K [34]) models, respectively. It was found that at low temperatures the scattering by acoustic phonons dominates while at relatively high temperatures (T > 100 K) the optical phonons produce the main contribution [10, 34].

The values of the Debye characteristic temperatures obtained from the temperature dependence of the conductivity are in good agreement with the one from low-temperature (T = 2–10 K) specific-heat (SH) measurements Θ_D^{SH} = 327 K [9] (in [8] the value of 460±10 K has been reported). Let us point out that there is a big difference between the values of the Debye temperatures from ultrasonic Θ_D = 528 K [12] and rectangular-parallelepiped-resonance (RPR) measurements Θ_D = 544 K [13] compared to the ones from resistivity Θ_D = 327–330 K [9, 10] and specific heat Θ_D = 327 K [9]. We believe that this difference is due to the overestimated number of modes used in the calculations [12, 13]. If one takes into account that only three acoustic modes contribute to elastic constants, the Debye temperature Θ_D becomes equal to 320–360 K in good agreement with results from other works [2, 9, 10]. To make a comparison between the specific-heat measurements and XRD or EXAFS results, it is necessary to have Θ_D^{SH} values measured at temperatures $T \geqslant \hbar\omega_o/k_B$ where ω_o is the optical mode frequency. For ReO_3, if we relate ω_o to the lowest optical branch [11], the condition is $T \geqslant$ 380 K. Unfortunately, there has been no work published where such data are available.

It is known that the vibrational properties of ReO_3 are characterized by a high anisotropy both for oxygen atoms and for the whole crystal. Its acoustic properties are dominated by very strong rhenium–oxygen bonds leading to high anisotropy of the shear wave propagation [2, 12, 13]. Also XAS [38] and x-ray structural analysis of the charge densities in ReO_3 [3] indicate an anisotropic charge distribution around rhenium atoms and a high anisotropy of oxygen thermal vibrations: their amplitude is much smaller in the Re–O–Re direction than in the perpendicular one [3]. Such thermal behaviour is similar to the observations for many perovskite crystals where a displacive phase transition occurs due to optical mode softening at low temperatures [26]. Therefore the possibility of an analogous phenomenon in ReO_3 involving the oxygen displacements from perfect octahedral sites was suggested [12], but not confirmed at normal pressure down to liquid-helium temperature [15]. In the present work, it was found that in the temperature range from 77 to 350 K, there is no change of the Re–O distance detectable by EXAFS, and no local distortion of the ReO_6 octahedra is present. Such stability of the ReO_3 lattice can be explained in terms of its electronic structure [14, 15]. The electronic-structure calculations [39–41] show that in ReO_3 the highly covalent bonding between oxygen and rhenium atoms results (1) in the highly directional Re–O π bonds formed by O 2p and Re 5d(t_{2g}) electrons and (2) in the broadening of the 5d-like conduction band with one electron per rhenium leading to the high conductivity. Therefore the absence of a structural phase transition in ReO_3 is explained by the fact that the total crystal energy should increase when the crystalline lattice distortion causes the increase of the total energy of the conduction electrons [14, 15].

7. Summary and conclusions

The x-ray absorption spectra of the rhenium L_3 edge in ReO_3 have been measured in the temperature range from 77 to 350 K. The application of the Debye and Einstein vibrational models to the analysis of EXAFS and XRD data for compounds with different degrees of correlation in atomic motion has been discussed. The MSRDs for the first, fourth and sixth coordination shells, corresponding to the Re–O_1, Re–Re_4, Re–Re_6 atom pairs, have been extracted for the first time using the best-fit procedure of the EXAFS signal with experimental and theoretical backscattering amplitudes and phase shifts.

A strong rhenium–oxygen interaction has been detected for the nearest-neighbour rhenium and oxygen atoms leading to the high correlation of their motion. The optical phonons with Θ_E (table 1) near 800 K contribute mainly to the MSRD of the first shell.

The temperature dependences of the MSRD and MSD for Re–Re shells can be well explained by the Debye model with close characteristic temperatures Θ_D (table 1) near 350 K. These values for the Re–Re pairs are in good agreement with the ones obtained by other experimental techniques (table 2). The acoustic phonons contribute mainly to the MSRD of the Re–Re pairs.

No evidence of a phase transition due to optical mode softening has been observed from 77 to 350 K.

Acknowledgments

The authors are grateful to Professor E Burattini and the staff of the PWA laboratory for support during experiments. AK and JP wish to acknowledge the partial support of this work from the Centro CNR di Fisica degli Stati Aggregati ed Impianto Ionico (Trento) and the University of Trento. The work in Riga was supported by grant 20041 from the International Science Foundation.

References

[1] Biltz W, Lehrer G A and Meisel K 1932 *Z. Anorg. (Allg.) Chem.* **207** 113
Meisel K 1932 *Z. Anorg. (Allg.) Chem.* **207** 121
Biltz W 1933 *Z. Anorg. (Allg.) Chem.* **214** 225
[2] Benner R E, Brody E M and Shanks H R 1977 *J. Solid State Chem.* **22** 361
[3] Morinaga M, Sato K, Harada J, Adachi H, Ohba S and Saito Y 1983 *J. Phys. C: Solid State Phys.* **16** L177
[4] Wertheim G K, Mattheiss L F, Campagna M and Pearsall T P 1974 *Phys. Rev. Lett.* **32** 997
[5] Pearsall T P and Lee C A 1974 *Phys. Rev.* B **10** 2190
[6] Narath A and Barham D C 1968 *Phys. Rev.* **176** 479
[7] Greiner J D and Shanks H R 1972 *J. Solid State Chem.* **5** 262
[8] Zumsteg F C and Pearsall T P 1975 *Solid State Commun.* **16** 751
[9] King C N, Kirsch H C and Geballe T H 1971 *Solid State Commun.* **9** 907
[10] Tanaka T, Akahane T, Bannai E, Kawai S, Tsuda N and Ishizawa Y 1976 *J. Phys. C: Solid State Phys.* **9** 1235
[11] Ishii M, Tanaka T, Akahane T and Tsuda N 1976 *J. Phys. Soc. Japan* **41** 908
[12] Pearsall T P and Coldren L A 1976 *Solid State Commun.* **18** 1093
[13] Tsuda N, Sumino Y, Ohno I and Akahane T 1976 *J. Phys. Soc. Japan* **41** 1153
[14] Goodenough J B 1966 *J. Appl. Phys.* **37** 1415; 1971 *Prog. Solid State Chem.* **5** 145
[15] Fujimori A and Tsuda N 1980 *Solid State Commun.* **34** 433
[16] Balerna A, Bernieri E, Burattini E, Kuzmin A, Lusis A, Purans J and Cikmach P 1991 *Nucl. Instrum. Methods* A **308** 240
[17] Beni G and Platzman P M 1976 *Phys. Rev.* B **14** 1514

[18] Dalba G, Diop D, Fornasini P, Kuzmin A and Rocca F 1993 *J. Phys.: Condens. Matter* **5** 1643
[19] Kuzmin A, Purans J, Benfatto M and Natoli C R 1993 *Phys. Rev.* B **47** 2480
[20] Kuzmin A and Purans J 1993 *J. Phys.: Condens. Matter* **5** 2333
[21] Kuzmin A and Purans J 1993 *J. Phys.: Condens. Matter* **5** 267
[22] Koningsberger D C and Prins R (ed) 1988 *X-Ray Absorption: Principles, Applications, Techniques of EXAFS, SEXAFS and XANES* (New York: Wiley)
[23] Schaich W L 1976 *Phys. Rev.* B **14** 4420
[24] Rehr J J, Mustre de Leon J, Zabinsky S I and Albers R C 1991 *J. Am. Chem. Soc.* **113** 5135
[25] Mustre de Leon J, Rehr J J, Zabinsky S I and Albers R C 1991 *Phys. Rev.* B **44** 4146
[26] Ashcroft N W and Mermin N D 1976 *Solid State Physics* (Philadelphia, PA: Saunders)
[27] Chang T S and Trucano P 1978 *J. Appl. Crystallogr.* **11** 286
[28] Dalba G, Fornasini P and Rocca F 1993 *Phys. Rev.* B **47** 8502
[29] Sevillano E, Meuth H and Rehr J J 1979 *Phys. Rev.* B **20** 4908
[30] Böhmer W and Rabe P 1979 *J. Phys. C: Solid State Phys.* **12** 2465
[31] Gabrusenoks J 1983 *Izv. Akad. Nauk LSSR, Ser. Fiz. Tech. Sci.* **1** 66 (in Russian); 1979 *Izv. Akad. Nauk LSSR, Ser. Fiz. Tech. Sci.* **3** 90 (in Russian)
[32] Axe J D, Fujii Y, Batlogg B, Greenblatt M and Di Gregorio S 1985 *Phys. Rev.* B **31** 663
[33] Miyanaga T and Fujikawa T 1994 *J. Phys. Soc. Japan* **63** 1036
[34] Allen P B and Schulz W W 1993 *Phys. Rev.* B **47** 14 434
[35] Salje E, Gehlig R and Viswanathan K 1978 *J. Solid State Chem.* **25** 239
[36] Daniel M F, Desbat B, Lassegues J C, Gerand B and Figlarz M 1987 *J. Solid State Chem.* **67** 235
[37] Dickens P G, Birtill J J and Wright C J 1979 *J. Solid State Chem.* **28** 185
[38] Kuzmin A 1994 *J. Phys.: Condens. Matter* **6** 5761
[39] Mattheiss L F 1969 *Phys. Rev.* **181** 987; 1970 *Phys. Rev.* B **2** 3918; 1972 *Phys. Rev.* B **6** 4718
[40] Myron H W, Gupta R P and Liu S H 1973 *Phys. Rev.* B **8** 987
[41] Tsukada M, Tsuda N and Minami F 1980 *J. Phys. Soc. Japan* **49** 1115